NASA Contractor Report 3628

A Nonlinear Structural Concept for Compliant Walls

Edward L. Reiss

CONTRACT NAS1-14717
OCTOBER 1982

NASA

NASA Contractor Report 3628

A Nonlinear Structural Concept for Compliant Walls

Edward L. Reiss
Applied Institute of Mathematics, Inc.
Evanston, Illinois

Prepared for
Langley Research Center
under Contract NAS1-14717

National Aeronautics
and Space Administration

**Scientific and Technical
Information Branch**

1982

A NONLINEAR STRUCTURAL CONCEPT FOR COMPLIANT WALLS

Edward L. Reiss
Applied Institute of Mathematics, Inc.
Evanston, IL 60201

SUMMARY

Two mechanisms of drag reduction for flow over flat plates are investigated. The first mechanism employs Bushnell's hypothesis that compliant walls produce drag reduction by interfering with the formation and bursting of the turbulent spots in a turbulent boundary layer. It is shown that the required amplitudes and frequencies of the wall motion might be achieved by using slightly curved walls and the resulting large amplitude motions of snap buckling of the walls. A simple structural model of an arch is used in the analysis. It is shown from the exact solution of the arch problem that the required structural motions can be obtained for compliant walls constructed from materials like mylar. In obtaining the solution, a new asymptotic method, which we call the method of rational functions, was developed for analyzing jump phenomena. In the second mechanism the delay of transition from laminar to turbulent flow by driven walls is studied. It is shown for Poiseuille channel flow whose walls are driven by a periodic traveling wave that a significant increase in the transitional Reynolds number is obtained by appropriately prescribing the wave length and phase velocity of the wall motion. Previously developed asymptotic methods are used in the analysis.

1. Introduction

Nearly one-half of the total drag of high-subsonic speed, long range aircraft, is a result of viscous drag caused by turbulent skin friction. Thus, any method that substantially reduces this drag will dramatically effect future aircraft design, and the general question of energy conservation.

In a series of pioneering experiments Kramer, see e.g. [1] , demonstrated that significant drag reduction can be achieved in the motion of bodies under water by coating their surfaces with compliant materials. Kramer's most successful experiments occurred for compliant materials that attempted to simulate the skins of dolphins. The precise mechanism for the reduction of drag by compliant surfaces is not known. Kramer, and other investigators conjectured that the drag reduction resulted from a delay in transition from laminar to turbulent flow. However, it is presently believed that this effect is unimportant at the large Reynolds numbers in Kramer's experiments. Subsequent experiments on drag reduction by Russian scientists, see e.g. [2], substantiated and developed Kramer's ideas. However, experimental results on drag reduction by compliant walls for air flows are inconclusive. A critical and detailed survey on compliant wall research is presented in [3] .

In the past decade, fundamental experimental advances have been made in understanding how turbulence is produced in a turbulent boundary layer. These experiments show that there is an organized sequence of flow events that give rise to boundary layer turbulence. The basic feature of turbulence producing flows is the formation and subsequent motion of fluid "bursts" near the wall. The experiments indicate that most of the turbulence and hence most of the drag, is produced during the formation of the bursts

and their eventual motion away from the wall. A discussion and summary of the burst formation process is given in [3] .

Bushnell [3,4] has conjectured that compliant walls produce drag reduction by interfering and altering the bursting process. This mechanism requires the walls to respond with sufficiently large amplitude, and sufficiently high frequency. A variety of compliant walls have been employed using different materials and different structural configurations. They are described in [3,4,5] . However, none of these walls have provided the required motions, or resulted in significant drag reductions for air flows.

In this report, we present a new mechanism to achieve the desired wall motion. It employs slightly curved walls subjected to external pressures, and the ensuing nonlinear, large amplitude motion of the wall. That is, it relies on the dynamics of snap-buckling of curved elastic plates. To demonstrate this mechanism, we consider a shallow elastic arch, or equivalently a wide curved elastic plate, whose axis is aligned with the flow direction. To simplify the problem, we neglect the interaction of the arch with the air flow, and assume that a prescribed static pressure is applied to the surface of the arch. A further simplification is made by assuming that the undeformed shape of the arch, the pressure, the disturbances, and the response, vary sinusoidally in space. Then it is possible to solve the resulting differential equations exactly.

We show in Section 3, that as the pressure increases from zero, the arch assumes stable, static equilibrium states with relatively small amplitudes. They are called unbuckled states. At a critical value of the pressure, the unbuckled state becomes unstable because there are no nearby

equilibrium states for pressures slightly greater than the critical value. Then due to any small disturbance, the shell jumps, or snap buckles, resulting in a large amplitude periodic motion. This motion is obtained in Section 5, in terms of the geometrical and material parameters of the arch, and the amplitudes of the fluid-imposed disturbances.

In Section 6, we apply these results and show that for experimentally feasible arch geometries, and for certain materials like mylar, the amplitudes and frequencies of the motion are within the limits required by Bushnell's hypothesis for drag reducing compliant walls. However, the theory we have presented is not yet complete, because it was assumed that the fluid and arch motions are decoupled. Hence this theory does not account for the coupling or give a specific mechanism for transferring energy from the fluid flow to the arch to maintain the desired periodic motion. A more refined theory is required, which accounts for the fluid-solid interaction.

The asymptotic expansion, in terms of rational functions, of the exact solution that is obtained in Section 5, suggests a new asymptotic method for analyzing jump phenomena like, snap buckling, combustion, and population explosions. Standard asymptotic and perturbation methods are not applicable, because in jump phenomena the order of magnitude of the solution changes during the jump. The new method, which we call the method of rational functions has been presented in [6,7] .

Experiments with boundary layer flows over flat plates suggest that the delay of transition and drag reduction can occur by suitably driving the flat plate with a traveling wave, see e.g. [2,8,9]. We have considered the mathematically simpler problem of Poiseuille channel flow with driven walls [10]. The results are summarized in Section 7, where we show that transition from the laminar Poiseuille flow can be delayed by suitably

varying the phase velocity of the wall. Previously developed [11,12] asymptotic methods were employed in the analysis.

2. Formulation of the Dynamic Snapping of an Elastic Arch

A shallow elastic arch of length L, cross-sectional area A, and cross-sectional moment of inertia I, is subjected to a lateral force per unit length P(X,T). Here X is the axial coordinate of the arch, $0 \leq X \leq L$, and T is the time. The vertical position of the undeformed arch is $Y = W^o(X)$, where W^o is a specified function. If the deformed position of the arch is denoted by $Y = y(X,T)$, then the "excess" vertical displacement W(X,T) is defined by

$$W(X,T) \equiv W^o(X) - y(X,T) \quad . \tag{2.1}$$

We now define the following dimensionless variables and parameters,

$$\begin{aligned} &x \equiv X/L \quad , \quad t \equiv \frac{\pi^2}{2L}(E/\rho)^{1/2}T \quad , \quad w(x,t) = W(X,T)/L \quad , \\ &p(x,t) \equiv \left(\frac{2}{\pi^2}\right)\frac{2L}{EA}P(X,T) \quad , \quad w^o(x) = W^o(X)/L \quad , \end{aligned} \tag{2.2}$$

where ρ and E are the mass density per unit length and the Young's modulus of the arch, respectively. In terms of these variables, the initial boundary value problem for the arch is [13,14],

$$w_{xxxx} - sw_{xx} + [\pi^4/(4\ell)]w_{tt} = -sw^o_{xx} + [\pi^4/(4\ell)]p \quad , \tag{2.3a}$$

$$s(t) \equiv (\ell/2)\int_0^1 (w_x^2 - 2w_x^o w_x)dx \quad , \tag{2.3b}$$

$$w = w_{xx} = 0 \quad , \quad \text{for } x = 0,1 \quad , \tag{2.3c}$$

$$w(x,0) = f(x) \quad , \quad w_t(x,0) = g(x) \quad , \tag{2.3d}$$

where the dimensionless parameter ℓ is defined by

$$\ell \equiv L^2 A/I \quad . \tag{2.4}$$

The quantity s(t) that is defined in (2.3b) is the dimensionless axial stress in the arch. It is independent of x. The boundary conditions (2.3c) imply that the ends of the arch, x = 0,1 are simply supported. The prescribed functions f(x) and g(x) are the dimensionless initial vertical displacement and initial vertical velocity of the arch, respectively.

We analyze (2.3) for sinusoidal arches, with sinusoidal initial data, and static but spatially sinusoidal pressures. Thus we have

$$w_0 = h \sin \pi x \quad , \quad p = q \sin \pi x \quad , \tag{2.5a}$$

$$f = f_0 \sin \pi x \quad , \quad g = g_0 \sin \pi x \quad , \tag{2.5b}$$

where h is the dimensionless maximum arch rise and q is the dimensionless maximum pressure. Then (2.3) and (2.5) has solutions

$$w(x,t) = A(t) \sin \pi x \quad , \tag{2.6}$$

where A(t) is the excess vertical displacement at the center of the arch, and it satisfies the initial value problem,

$$\begin{aligned} &A'' + \alpha A - 3hA^2 + A^3 - q = 0 \quad , \\ &A(0) = f_0 \quad , \quad A'(0) = g_0 \quad . \end{aligned} \tag{2.7}$$

A prime denotes differentiation with respect to t, and the parameter α is defined by

$$\alpha \equiv 2(h^2 + 2\ell) \quad . \tag{2.8}$$

3. The Static States

It follows from (2.7) that the amplitudes of the single mode equilibrium positions of the arch satisfy the cubic equation,

$$q = \alpha A - 3hA^2 + A^3 \quad . \tag{3.1}$$

We refer to, (3.1) as the static response equation, and to its graph as the static response curve.

The number of real roots of (3.1) depends on the sign of the discriminant,

$$D \equiv h^2 - \alpha/3 = \frac{(h^2 - 4\ell)}{3} \quad . \tag{3.2}$$

We consider only arches with $D > 0$. Then there is a unique static state for q in the intervals $q < q_\ell$, and $q > q_u$, see Fig. 1. However, for q in the interval $q_\ell < q < q_u$, there are three static states. The lower branch of this curve, with amplitudes in the range, $0 \leq A \leq A_u$, is called the unbuckled branch. The upper branch ($A \geq A_\ell$) is called the buckled branch. The remaining states with amplitudes in the interval, $A_u \leq A \leq A_\ell$, lie on the intermediate branch.

As q increases from zero, the equilibrium states of the arch lie on the unbuckled branch. If q exceeds q_u, then the arch must jump dynamically towards the buckled state. Similarly if the arch is in an equilibrium state corresponding to a point on the buckled state, and q is slowly decreased below q_ℓ, the arch will suddenly jump towards the unbuckled state. These dynamic transitions are called snap buckling. They are described by the initial value problem (2.7) for disturbances given by (2.5b).

Consequently the dimensionless pressure q_u and q_ℓ are called the upper and lower buckling loads, respectively. Their values are easily obtained from an elementary analysis of (3.1) as,

$$q_u = 4h\ell + 2D^{3/2} \quad , \quad q = 4h\ell - 2D^{3/2} \quad . \tag{3.3}$$

The corresponding values of the amplitudes are,

$$A_u = h - D^{1/2} \quad , \quad A_\ell = h + D^{1/2} \quad . \tag{3.4}$$

The amplitude of the buckled state, $A_b(q_u)$, corresponding to $q = q_u$ is obtained from (3.1) as

$$A_b(q_u) = 3h - 2A_u = h + 2D^{1/2} \quad . \tag{3.5}$$

The stability of the equilibrium states to single mode disturbances of the form (2.5b) is determined by linearizing (2.7) about any equilibrium state $A = A_e$. From an analysis of this linearized problem, we conclude that the unbuckled and buckled branches are stable, and the intermediate branch is unstable. In addition, the limit points, $q = q_u$, $A = A_u$, and $q = q_\ell$, $A = A_\ell$, are unstable equilibrium states. We wish to study the motion that results (snapping) when the arch is given a small disturbance from the equilibrium state corresponding to a limit point.

4. The Phase Plane Analysis

The qualitative features of the dynamic motion of the arch will now be obtained from a phase analysis of (2.7). The system (2.7) describes the oscillations of a conservative mechanical system. The phase plane diagram is sketched in Figure 2, for $D > 0$, and q in the interval $q_\ell < q < q_u$, where $A_1(q)$, $A_2(q)$, and $A_3(q)$ are the amplitudes of the equilibrium states corresponding to the unbuckled, intermediate, and buckled branches, respectively. Each trajectory is characterized by a value of the initial energy of the system.

The equilibrium points A_1 and A_3 are centers in the phase plane, and the unstable equilibrium point A_2 is a saddle. The closed curves surrounding $A_1(A_3)$ and lying inside the separatrix in Figure 2 represent periodic oscillations of the arch about the unbuckled (buckled) equilibrium state. The closed curves lying outside of the separatrix and enclosing all three equilibrium points in their interior, represent large amplitude periodic motions of the arch swaying back and forth between the unbuckled and buckled states. It is the latter, large amplitude motion that is of particular interest for drag reduction structures.

As $q \to q_u$, the equilibrium states A_1 and A_2 coalesce to form the limit point. In the phase plane, the center and the saddle coalesce to form a new singular point, which is a cusp. The resulting phase plane diagram is sketched in Figure 3. The closed curves surrounding both equilibrium points, and lying outside the separatrix, represent large amplitude, periodic motions of particular interest because they correspond to the snap buckling of the arch.

It is possible to calculate the local periodic motions about A_1 and A_3 in Figure 2, and A_3 in Figure 3 by the Poincare-Linstedt [15] perturbation method. Since our primary interest is in the large amplitude motion of the arch, this method is not applicable. In the next section, we determine the snap buckling motion by solving (2.7) exactly in terms of elliptic functions. Then an expansion of the resulting solution is obtained for small initial disturbances from the limit point. This suggests a new asymptotic method for analyzing jump phenomena. This new method, which we call the Method of Rational Functions, is described in [6,7].

5. The Dynamics of Snap Buckling

To analyze the snap buckling of the arch, we assume that $q = q_u$ and the arch is in equilibrium at the limit point, $A = A_u$. A small initial displacement disturbance ε is given to the arch, so that,

$$A(0) = A_u + \varepsilon \quad , \quad A'(0) = 0 \quad . \tag{5.1}$$

The ensuing large amplitude periodic motion describes the snap buckling of the arch. In our analysis, we assume that $\varepsilon < 0$. A similar analysis applies for $\varepsilon > 0$. Then the motion is periodic, but it lies on a closed curve inside the separatrix in Figure 3.

It is convenient to transform the dependent variable in (2.7), to analyze the motion relative to the limit point. Thus, we define v(t) by

$$A(t) = A_u + v(t) \quad . \tag{5.2}$$

By inserting (5.1), (5.2), and $q = q_u$ into (2.7), the initial value problem is transformed to,

$$v'' - 3D^{1/2}v^2 + v^3 = 0 \quad , \quad v(0) = \varepsilon \quad , \quad v'(0) = 0 \quad , \tag{5.3}$$

where the parameter D is defined in (3.2). The phase plane diagram for (5.3) is the same as Figure 3 with the origin shifted to the limit point.

By integrating the first integral of (5.3), we obtain a representation of the solution of (5.3) in terms of the elliptic function

$$\phi(\tau) \equiv \cos \tau \tag{5.4}$$

and the roots of a quartic equation, see [6] for details. For small ε the roots are obtained by a perturbation method. This leads to the representation

$$v(t;\varepsilon) = \frac{\delta(\tfrac{1}{2} - \sqrt{3})\left[1 + \left(\frac{1 + \sqrt{3})}{1 - \sqrt{3})}\right)\phi(\tau)\right]\varepsilon + O(\varepsilon^2)}{[1+\phi(\tau)] + (\tfrac{1}{2} - \sqrt{3})\left[1 + \left(\frac{\frac{1}{2} + \sqrt{3}}{\frac{1}{2} - \sqrt{3}}\right)\phi(\tau)\right]\varepsilon + O(\varepsilon^2)} \quad . \tag{5.5}$$

where the parameter δ is defined by $\delta \equiv 4D^{1/2}$, and

$$\tau = \left[\left(\frac{\sqrt{3}\,\delta}{2}\right)^{1/2}(-\varepsilon)^{1/2} + \cdots\right]t \quad . \tag{5.6}$$

The function $\phi(\tau)$ is periodic of period $4K$, where $K(k)$ is the complete elliptic integral of the first kind with modulus k. The modulus is given by

$$k^2 = \left(\frac{2 + \sqrt{3}}{4}\right) + O(\varepsilon) \quad . \tag{5.7}$$

From tables of the complete elliptic integral of the first kind [16] we get,

$$K(k) \backsimeq K_0 + O(\varepsilon) \text{ , where } K_0 = K\left(\frac{2 + \sqrt{3}}{4}\right) \backsimeq 2.7693 \quad . \tag{5.8}$$

It follows from (5.5) and (5.6) that the period of the motion is

$$t_0 = 4\sqrt{2}K/(BE)^{-1/2} = \frac{4\sqrt{2}K_0}{3^{1/4}\delta^{1/2}}(-\varepsilon)^{-1/2} + O(1) \quad . \tag{5.9}$$

The mathematical structure of the snap buckling of the arch, and perhaps other jump phenomena, where the solution changes from small $[O(\varepsilon)]$ to large $[O(1)]$, is revealed by the rational functions (5.5). Since $1 + \phi(\tau) = 0$ only for $\tau = \tau_n(\varepsilon) \equiv 2(1 + 2n)K$, $n = 0,1,2,\cdots$, the leading term in the denominator, $1 + \phi(\tau)$, does not vanish for τ in the interval, $\tau_n < \tau < \tau_{n+1}$. Hence, the denominator changes from $O(1)$ to $O(\varepsilon)$, and then back to $O(1)$ as τ varies through τ_n. Since the numerator is $O(\varepsilon)$, the solution jumps from $O(\varepsilon)$ to $O(1)$ and back to $O(\varepsilon)$ as τ varies through τ_n. The jump occurs smoothly, but rapidly. That is, the solution remains $O(\varepsilon)$ for most of the period, and jumps to $O(1)$ and returns to $O(\varepsilon)$ over a

relatively short interval of time. The period of the motion is long, as we deduce from (5.9).

If the Poincaré-Linstedt method is applied to (5.3), the leading term is given by (5.5), with only the O(1) term in the denominator. Thus, the approximation given by this method is unbounded at $\tau = \tau_n$, n = 0,1,..., and hence it is invalid.

6. Application to Drag Reduction Compliant Walls

For an arch of rectangular cross-section of breadth b and depth d, the parameters ℓ and D that are defined in (2.4) and (3.2), respectively, are given by

$$\ell = (1/12)(d/L)^2 \quad , \quad D = \frac{1}{3}\left[(H/L)^2 - (1/3)(d/L)^2\right] \quad . \tag{6.1}$$

Here $H = W^o(L/2)$ is the arch rise, i.e. it is the physical height of the center of the undeformed arch above the horizontal.

In physical variables, the pressure P_u and the static displacement W_u at the center of the arch corresponding to the limit point q_u, A_u are

$$\frac{P_u}{b} = \frac{\pi^4}{4}\frac{EA}{bL}q_u = \frac{\pi^4 E}{4}\left[\left(\frac{d}{L}\right)\frac{1}{3}\left(\frac{H}{L}\right)\left(\frac{d}{L}\right)^2 + 2D^{3/2}\right] \quad ,$$

$$W_u = Lw_u(1/2) = LA_u = L\left[\frac{H}{L} - D^{1/2}\right] \quad . \tag{6.2}$$

We have used (2.2), (2.6), (3.3) and (3.4) to obtain (6.2). Similarly, the physical displacement W_b at the center of the static buckled arch for $q = q_u$ is obtained from (3.5) and (2.2) as,

$$W_b = LA_b = L\left[\frac{H}{L} + 2D^{1/2}\right] \quad . \tag{6.3}$$

The maximum displacement W_m of the arch during the motion is evaluated from (5.5) and (3.4) as

$$W_m = L\left[\frac{H}{L} + 3D^{1/2} + O(\varepsilon^3)\right] \quad . \tag{6.4}$$

Finally, the period T_0 in seconds of the large amplitude motion, with $q = q_u$, is obtained by inserting the time scaling in (2.2) into (5.9). This gives,

$$T_0 = \frac{2L}{\pi^2}(\rho/E)^{1/2} t_0 = \frac{4\sqrt{2}K_0 L}{\pi^2 3^{1/4} D^{1/4}}\left(\frac{\rho}{E}\right)^{1/2}(-\varepsilon)^{-1/2} + O(1)$$

$$\approx \frac{1.206L}{D^{1/4}}\left(\frac{\rho}{E}\right)^{1/2}(-\varepsilon)^{-1/2} + O(1) \quad . \tag{6.5}$$

Typical dimensions (in inches) of panels used in drag reduction experiments [3]-[5] are,

$$.02 \leq L \leq .035 \quad , \quad .002 \leq H \leq .003 \quad ,$$

$$.0001 \leq d \leq .01 \quad . \tag{6.6a}$$

Then the parameters (H/L), (d/L), and D lie in the intervals,

$$.07 \leq H/L \leq .15 \quad , \quad .005 \leq d/L \leq .286 \quad ,$$

$$0 < D \leq .0075 \quad . \tag{6.6b}$$

For (H/L) large compared to (d/L), then D, and the quantities in (6.2)-(6.5) are given approximately by

$$D \approx \frac{1}{3}(H/L)^2 \quad , \quad \frac{P_u}{b} \approx \frac{\pi^4}{6\sqrt{3}} E\left(\frac{d}{L}\right)\left(\frac{H}{L}\right)^3 \quad , \quad T_0 \approx \frac{1.587L\sqrt{\rho/E}}{\sqrt{H/L}\sqrt{-\varepsilon}} + O(1) \quad ,$$

$$W_u \approx \frac{\sqrt{3}-1}{\sqrt{3}} H \quad , \quad W_b \approx \frac{\sqrt{3}+2}{\sqrt{3}} H \quad , \quad W_m \approx (1+\sqrt{3})H \quad . \tag{6.7}$$

Thus W_b and W_m are approximately 5 and 6.5 times larger, than W_u, respectively if (H/L) >> (d/L).

If we denote the height of the arch at maximum displacement by H_m, then we obtain from (6.4)

$$H_m = H + W_m = 2H + 3LD^{1/2} + O(\varepsilon) \tag{6.8}$$

By substituting the maximum values of H, L and D given in (6.6) into (6.8), we obtain for the maximum value of H_m

$$H_m \lesssim .015 \text{ inches} \quad . \tag{6.9}$$

Significantly smaller values of H_m are obtained for other values of H, L and D in the ranges given in (6.6). For example, if H/L is large compared to d/L then using (6.7) in (6.8) we obtain

$$H_m \lesssim (2 + \sqrt{3})H \quad . \tag{6.10}$$

Then by using the minimum value of H from (6.6a), we get $H_m \lesssim .0075$ inches from (6.9). It is conjectured [3] that wall motions with relatively large amplitudes are necessary for drag reduction. In experiments conducted at Langley with other compliant wall structures and mechanisms, it was difficult to excite motions with amplitudes as small as .0008. The present analysis suggests that amplitudes ten to twenty times larger can be obtained using the snap-buckling of curved structures.

If the maximum amplitudes of compliant walls are too large, they will induce drag because of a "roughness" effect. For turbulent boundary layer flows, an empirical rule is that the maximum amplitudes should not exceed $100\ \nu/U_\infty$, where ν is the kinematic viscosity of the fluid and U_∞ is the free stream velocity of the flow [21]. For the typical experimental values of $\nu = 1.5 \times 10^{-4}$ ft^2/sec. and U_∞ in the range, 3 ft/sec $\leq U_\infty \leq$ 25 ft/sec, the empirical rule requires that the maximum amplitudes lie between .0072 inches and .06 inches for a hydraulically smooth surface. The geometrical parameters H, L and D can be selected so that the maximum amplitudes lie within these values.

It has been conjectured from experiments and a study of data, see e.g. [3], that wall frequencies $T_0^{-1} \simeq 2000$ Hertz are necessary for drag reduction. For this frequency, we conclude from (6.5) that the corresponding amplitude ε of the disturbance is given approximately by,

$$-\varepsilon \simeq 582 \times 10^4 (\rho/E) L^2/D^{1/2} \quad . \tag{6.11}$$

In Table 1, we give the values of $-\varepsilon$ obtained from (6.10) for typical materials used in drag reduction studies. The values of ρ/E were obtained from [5].

To interpret the results in Table 1, we recall that ε represents a small displacement disturbance applied to the arch. We observe from the table that at a frequency of 2000 Hertz, mylar would be a suitable material for a wide range of the geometric parameter $L^2/D^{1/2}$. That is, small disturbances can produce a periodic motion at the required frequency. The materials 100 PPI foam and RTV are suitable provided that $L^2D^{1/2}$ is sufficiently small. Other materials such as PVC that have been used in drag reduction experiments are unsuitable because they require a relatively large value of $-\varepsilon$ to excite the periodic motion with the required frequency.

Criteria for selecting the magnitude of ε are not given by the present theory. The parameter ε crudely represents disturbances produced by air flow over the arch, such as turbulent boundary layer fluctuations. If the magnitude of these fluctuations is known, or can be measured in an experiment, then, by using the analysis and results of the present investigation, it is possible to crudely estimate the geometric and material properties of the arch that are necessary to produce the desired frequency and amplitude of response. These results apply only to initial disturbances of the

form (2.5b). If more complicated disturbances occur then the response will contain more than one mode. Additional modes introduce more equilibrium states of the arch than are illustrated in Figure 1, see e.g. [14].

Aerodynamic and structural damping have been neglected in the formulation (2.3). The presence of a small amount of structural damping will change the center at A_3 in Figure 3 to a stable spiral point. Then instead of snap buckling occurring as a periodic oscillation, there will be a damped oscillation with the solution approaching the buckled equilibrium state at A_3 as $t \to \infty$. That is, energy is lost by the system due to structural damping, and the arch eventually comes to rest at the buckled equilibrium point. In order to maintain a periodic oscillation, energy must be supplied to the arch from its environment, to replace the energy lost by dissipation. This energy may be obtained from the pressure induced by aerodynamic forces, and from turbulent boundary layer fluctuations. For example, the turbulent boundary layer fluctuations may provide sufficient disturbances to the arch at regular intervals to continually excite a periodic, or nearly periodic, large amplitude oscillation. However, the aerodynamic forces may also damp the motion. A more sophisticated study is required to determine whether the net energies supplied to the arch by the aerodynamic pressures and turbulent boundary fluctuations are sufficient. Then it is necessary to consider the coupled aerodynamic-structural interaction problem.

7. Poiseuille Channel Flow with Driven Walls

The flow of a viscous, incompressible fluid between two horizontal, rigid and infinite walls that is driven by a horizontal pressure gradient is called Poiseuille channel flow. It is described mathematically by an initial-boundary value problem for the two-dimensional Navier-Stokes equations. Plane Poiseuille flow is a laminar flow solution of this problem for all values of R. The Reynolds number that characterizes the flow is $R \equiv U_0 H/\nu$. Here, 2H is the channel gap*, ν is the kinematic viscosity and U_0 is the centerline velocity of this flow.

It follows from the linearized theory of hydrodynamic stability [17] that plane Poiseuille flow is stable (unstable) for $R < R_c$ ($> R_c$). The critical Reynolds number, R_c, is determined numerically as, $R_c \backsimeq 5772$, see e.g. [18]. In addition, a branch of unstable spatially and temporally periodic solutions of the Navier-Stokes problem bifurcates subcritically from the laminar flow solution at $R = R_c$ [19]. Thus, $R = R_c$ is a bifurcation point of plane Poiseuille flow.

In [10] we have modified this classical channel flow problem by driving the upper wall with a specified vertical motion to determine if transition can be delayed to a Reynolds number $> R_c$. In the dimensionless variables

$$x \equiv X/H \quad , \quad y \equiv Y/H \quad , \quad t \equiv (U_0/H)T \quad , \tag{7.1}$$

the wall motion is given by

$$y = 1 + \delta G(x,t) \quad , \quad G(x,t) \equiv \cos(\alpha x - ct) \quad . \tag{7.2}$$

Thus, $\delta G(x,t)$ is a traveling wave of amplitude δ and phase velocity c/α, where α and c are the dimensionless wave number and circular frequency, respectively. For simplicity of presentation, we assume that $\delta \geq 0$. In

*This H should not be confused with the maximum arch rise of Sections 2-6.

terms of a dimensionless stream function $\Psi(x,y,t)$, the two dimensional Navier-Stokes equations are reduced to

$$\Delta\Psi_t - \frac{1}{R}\Delta^2\Psi + J(\Psi,\Delta\Psi) = 0 \quad . \tag{7.3a}$$

Here Δ and Δ^2 are the two dimensional harmonic, and biharmonic operators, respectively. The nonlinear operator J is defined for any two functions f, and g by

$$J(f,g) \equiv f_y g_x - f_x g_y \quad . \tag{7.3b}$$

The boundary conditions on the walls are,

$$\Psi_x(x,-1,t) = \Psi_y(x,-1,t) = 0 \tag{7.3c}$$

$$\Psi_x(x,1 + \delta G(x,t),t) = -\delta G_t(x,t) \quad , \quad \Psi_y(x,1 + \delta G(x,t),t) = 0. \tag{7.3d}$$

The boundary conditions as $|x| \to \infty$ are,

$$\Psi(x,y,t), \text{ and its derivatives, are bounded as } |x| \to \infty \quad . \tag{7.3e}$$

For the dependence of the wall motion on the Reynolds number, we assume that,

$$c = c_0 + w\left(\frac{1}{R} - \frac{1}{R_c}\right) + O\left(\left(\frac{1}{R} - \frac{1}{R_c}\right)^2\right) \quad , \tag{7.3f}$$

where c_0 and w are parameters to be specified. For simplicity of presentation, the wave number α is assumed to be independent of R. The perturbed problem that we analyze is to determine solutions of (7.3) that are periodic in x with wave length $2\pi/\alpha$, and periodic in t with period $2\pi/c$. The perturbed problem is a forced oscillation problem, where the wall motion is the "forcing function". Thus, we are seeking solutions with the same period as the forcing function.

The classical hydrodynamic stability problem of Poiseuille channel flow is obtained by setting $\delta = 0$ in (7.3). We refer to the problem of determining periodic solutions of periods $2\pi/\alpha$ in x, and $2\pi/\omega$ in t, of (7.3) with $\delta = 0$ as the bifurcation problem. Here, the wave number α, and the circular frequency ω are to be determined. The bifurcation problem possesses the laminar flow solution,

$$\Psi = \Psi^0 \equiv y - y^3/3 \quad , \tag{7.4}$$

for all values of R, and $\alpha = \omega = 0$. It is the classical plane Poiseuille flow. In the terminology of bifurcation theory, it is the basic solution of the bifurcation problem.

The stability of the basic solution (7.4) is determined by linearizing (7.3) with $\delta = 0$, about the basic solution. Solutions of the resulting problem are obtained in the form,

$$\Psi = e^{-\zeta t} e^{ikx} \phi(y) \quad , \tag{7.5}$$

where the wave number k is real. Then ζ, and ϕ are determined as the eigenvalues $\zeta_j(k,R)$, and the eigenfunctions, $\phi_j(y;k,R)$ of the Orr-Sommerfeld problem [17].

We have employed a modified version of the Chebyschev method [18] to solve the Orr-Sommerfeld problem numerically. The resulting critical Reynolds number R_c, the wave number $k = k_c$, and the frequency $\omega = \omega_c$ at criticality are estimated as,

$$R_c \approx 5772.22 \quad , \quad k_c \approx 1.02056 \quad , \quad \omega_c \equiv \text{Im}\, \zeta_1 \approx .264002 \quad . \tag{7.6}$$

Here $\zeta_1(k,R)$ and $\phi_1(y;k,R)$ are the eigenvalue and eigenfunction corresponding to the lowest mode, and $\text{Re}\, \zeta_1(k_c,R_c) = 0$. In dimensional variables, the wavelength at criticality is approximately three times the channel depth. Thus, the laminar flow is stable for $R < R_c$, and it is unstable for $R > R_c$.

A generalization of the method presented in [11,12] was employed [10] to determine asymptotic expansions of the solutions of the perturbed problem (7.3) as $\delta \to 0$. These expansions are obtained as perturbations of the solutions of the bifurcation problem. Since these perturbations are singular, the method of matched asymptotic expansions is used in the analysis. We now give a brief summary of the results of this analysis. All details of the analysis are omitted; see [10] for details.

On the results for the resonance case, which is defined by,

$$\alpha = k_c \quad , \quad c(R_c) \equiv c_0 = \omega_c \quad , \tag{7.7}$$

are discussed in this report. The resulting solutions of the perturbed problem in the non-resonance cases are in general, quasi-periodic functions; see [10] for details. Asymptotic expansions of the solutions of the perturbed problem for R near R_c and in the resonance case are given by,

$$\Psi = \Psi^o + 2r(R)\mathrm{Re}\left\{ e^{i[k_c x-(\omega_c+w\xi\delta^{2/3})t-\theta+0(\delta)t]} \phi_1(y) \right\} \delta^{1/3} + 0(\delta^{2/3}) \quad , \tag{7.8}$$

where k_c and ω_c are given in (7.6), w is defined in (7.3f), $\phi_1(y)$ is the Orr-Sommerfeld eigenfunction, and ξ is defined by

$$R = R_c - R_c^2 \xi \delta^{2/3} + 0(\delta) \quad . \tag{7.9}$$

Thus, by varying ξ and w, the Reynolds number and the forcing frequency c are varied respectively near their critical values. The amplitude r, and the phase shift θ in (7.8) are the real roots of the amplitude equations,

$$r^3 + p\xi r = \pm(\gamma^2 - q^2\xi^2 r^2)^{1/2} \quad , \tag{7.10a}$$

$$\theta = \sigma + \sin^{-1}\left(\frac{q\xi r}{\gamma}\right) \quad . \tag{7.10b}$$

The quantities p, and q in (7.10) are linear functions of w that are numerically evaluated from integrals involving the Orr-Sommerfeld eigenfunction and its adjoint eigenfunction. They are given by,

$$p \eqsim 1.466825 - (.0056057)w \quad , \quad q \eqsim -.582325 + (.001004)w \quad . \tag{7.11}$$

The constants γ and σ in (7.10), which are evaluated similarly, are given by

$$\gamma \eqsim .000163 \quad , \quad \sigma \eqsim -.229238 \quad . \tag{7.12}$$

The response (7.8) is a small perturbation of the laminar flow Ψ^o. The amplitude of the perturbation is proportional to $r\delta^{1/3}$. Thus, the small disturbance, whose amplitude is proportional to δ, produces a much larger response. The exponential factor in (7.8) gives the propagation of the transverse normal mode ϕ_1 down the channel. Thus, the perturbation propagates with the same wave length in x and period in t as the impressed wall motion, but it is phase shifted by $\theta(R)$, see (7.3f) and (7.8). We refer to the solutions (7.8) as perturbed laminar states.

An elementary analysis of the amplitude equations (7.10) which we do not present, shows that there are four critical values of w. They are denoted by w_L, w_p, w_H, and w^*. The critical values w_p and w^* are the zeros of $p = 0$ and $q = 0$, respectively. The critical values $w_L < w_H$ are the two roots of

$$p^2(w) - 3q^2(w) = 0 \quad . \tag{7.13}$$

By using the values in (7.11) and (7.12), these critical values are given approximately by,

$$w_L \eqsim 116 \quad , \quad w_p \eqsim 262 \quad , \quad w_H \eqsim 338 \quad , \quad w^* \eqsim 585. \quad . \tag{7.14}$$

The critical values define five intervals of values of w where the response curves have different qualitative features. Typical response curves

for each of these intervals are sketched in Fig. 5. The perturbed laminar states have a maximum amplitude at $R = R_m$. The value of this maximum and its location depend on w, as illustrated in Fig. 4. As $w \to w^*$, $r_m \to \infty$ and $R_m \to \infty$. Thus, when $w = w^*$, the perturbed states give a continuous transition from the laminar state to the bifurcation state, as shown in Fig. 4e. The dotted curve in each of these figures is the solution of the bifurcation problem that branches from $R = R_c$.

The significance of the critical value w_p is that $R_m > R_c$ ($< R_c$) if $w < w_p$ ($> w_p$). At $w = w_p$, R_m and R_c coincide. For w in the open interval (w_L, w_H), the response curve gives the amplitude as a single valued function of R. For w outside this interval the response curves are multiple-valued. At $w = w_L$, and at $w = w_H$, the response curve has a vertical slope near $R = R_m$. Multi-valued response diagrams define two additional critical values of R. They are denoted by R_U, and R_L as shown in Fig. 4a. They are characterized as the points of vertical slope. Their values, which depend on w, are obtained directly from (7.10a).

The interpretation of the results depends on the stability of the solutions. For many nonlinear stability problems it can be shown that solutions are stable (unstable) if

$$\frac{dr}{dR} > 0 \quad (< 0) \quad . \tag{7.15}$$

That is, they are stable (unstable) if the amplitude of the response increases (decreases) with the Reynolds number. We shall discuss the results assuming that this statement is true. However, it is important to emphasize that the present analysis determines periodic solutions near the laminar state that have the same wavelength and frequency as the wall motion. They may be other periodic solutions of the perturbed problem, such as subharmonic

solutions. In addition, there may be other periodic, and non-periodic solutions of the initial value problem for the system (7.3). Since the precise long-time behavior of the solutions of this system is unknown, it is difficult to assess the significance of these additional solutions. In particular, the stability of a class of solutions of (7.3) was investigated in [20]. There the frequency of the wall motion was fixed at criticality, so that in the present notation, only the special case $w \equiv 0$ was considered. The Stuart-Watson method was employed leading to a first order, ordinary differential equation for the slow time variation of the complex valued amplitude. This equation possesses time independent solutions, which were shown to be stable for $R < R_1 < R_c$, and unstable for $R \geq R_1$. Thus, if the Stuart-Watson method provides a valid approximation to solutions of (7.3), then the analysis in [20] suggests the possibility of the bifurcation of additional periodic solutions at $R = R_1$. An investigation of the stability of the solutions (7.8) is currently in progress.

We first discuss the results for $w < w_p$; see Figs. 5a,b. Then as R increases from zero, the fluid is in a stable, perturbed laminar state. The amplitude of the wave increases until $R = R_m$. Any further increase in R results in an unstable state. This suggests that as R increases through R_m there is dynamic transition to another state of the fluid. This transition may be rapid and involve large amplitudes. However, if $w < w_L$, and $R = R_m$, then the solutions may execute a "small" amplitude jump from the upper branch in Fig. 5a to the stable intermediate branch with $r = r_I$. Then by further increasing R, a second transition will occur at $R = R_u$ to some other state of the fluid (possibly turbulent). It is important to boserve that for $w < w_p$, R_m, and hence R_u, exceed R_c. So that the jumps we have described occur when R exceeds R_c. That is, transition is delayed. The maximum

excursion of R_m to the right, and hence the largest delay occurs when $w \approx 180$, as is deduced from our analysis. The corresponding value of R_m is denoted by $\bar{R}_m$, and it is given by

$$\bar{R}_m = R_c[1 + 28.063\delta^{2/3} + 0(\delta)] \quad . \tag{7.16}$$

Then for the typical experimental value of $\delta = .002$, we obtain from (7.16) that $\bar{R}_m \approx 8344$. This gives a 45% increase in the transitional Reynolds number. Thus, wall motions provide a method for nonlinear stabilization. This interpretation may be of practical significance for the control of turbulence in channel, pipe and other viscous flows. Additional control of the transition might be achieved by oscillating the lower wall so that it is phase shifted with respect to the upper wall.

The stability of the fluid in the presence of the wall motion is determined by two competing physical effects. The wall motion disturbs the laminar flow, which tends to destabilize the fluid. However, the resulting motion is out-of-phase with the wall motion. If the phase shift is small then the disturbance effect of the wall wins, and there is early transition. However, if the phase shift is sufficiently large, then the instability is restrained by the wall motion. This is confirmed by the variation with w of the phase shift corresponding to $R = R_m$, see Fig. 5. The phase shifts are larger when R_m exceeds R_c, i.e. when $w < w_p$.

A paper describing the results of this investigation has been submitted for publication.

8. Concluding Remarks

Two mechanisms for drag reduction in the flow over a flat plate are considered. The first mechanism employs compliant walls and Bushnell's conjecture that compliant walls produce drag reduction by interfering with and altering the formation and motion of the fluid bursts in the turbulent boundary layer adjacent to the wall. Experiments indicate that most of the turbulence, and hence most of the drag associated with a turbulent boundary layer, is produced during the formation of these bursts and their motion away from the wall. The walls must respond with sufficiently large amplitude and sufficiently large frequencies to produce the required interference. The proposed mechanism employs slightly curved walls and relies on the large amplitude motions due to snap-buckling of curved elastic structures. The mechanism is demonstrated for a simpler problem for a shallow, curved, elastic arch. For a suitable pressure distribution the dynamic problem of the arch is solved exactly. Employing this exact solution, we show that for experimentally feasible arch geometries and for wall materials like mylar, the amplitude and frequencies of the motion are within the limits required by Bushnell's hypothesis. Our analysis of the snap-buckling mechanism is incomplete since the fluid and structural motions are assumed to be decoupled. A more refined theory that accounts for the interaction of the fluid with the structure is required to describe a mechanism of transferring energy from the fluid flow to the structure to maintain the desired wall motion.

The second mechanism is concerned with delaying the transition from laminar to turbulent flow along a wall by driving the wall. We have considered the related but simpler problem of Poiseuille channel flow

whose walls are driven by a periodic traveling wave. It is shown that by appropriately selecting the wave number and phase velocity of this traveling wave a significant delay in the transitional Reynolds number can be achieved. This delay occurs because of the phase shift of the resulting periodic fluid motion with respect to the prescribed wall motion. Additional investigations are required to determine if a similar delay in transition can be achieved for boundary layer flows over a driven wall. Recent experiments [8] suggest that this may be possible.

References

1. Kramer, M. O., "Hydrodynamics of the Dolphin," in Advances in Hydroscience, 2, Academic Press, 1965, p. 111; "The Drag Reduction of Fast Underwater Bodies with the Aid of an Artificial Dolphin Skin," in Jahrbuch der Deutschen Gesell. fur Luft-und Raumfahrt, Blenk and Schutz, Cologne, 1969, p. 102.

2. Merkulov, V.I. and Savchenko, Yu.I., "Experimental Investigation of Fluid Along a Traveling Wave," Bionika 4 (1970), pp. 95-104.

3. Bushnell, D. M., Hefner, J. N., and Ash, R. L., "Effect of Compliant Wall Motion on Turbulent Boundary Layers," Phys. of Fluids, 20 (1977), pp. 531-548.

4. Ash, R. L., Bushnell, D. M., Weinstein, L. M., and Balasubramanian, R., "Compliant Wall Surface Motion and Its Effect on the Structure of a Turbulent Boundary Layer," presented at the Fourth Biennial Symposium on Turbulence in Liquids, University of Missouri, Rolla (1975).

5. Fischer, M. C., Weinstein, L. M., Ash, R. L., and Bushnell, D. M., "Compliant Wall-Turbulent Skin-Friction Reduction Research," AIAA Paper No. 75-833 (1975), presented at the AIAA 8th Fluid and Plasma Dynamics Conference.

6. Reiss, E. L., "A New Asymptotic Method for Jump Phenomena," SIAM J. Appl. Math. 39 (1980), pp. 440-455.

7. Reiss, E. L., "Jump Phenomena," in Nonlinear Partial Differential Equations in Engineering and Applied Science, Ed. by R. L. Sternberg, A. J. Kalinowski, J. S. Papadakis, Marcell-Dekker, Inc., N.Y., 1980, pp. 415-428.

8. Milling, R. N., "Tollmien-Schlichting Wave Cancellation," Phys. Fluids 24 (1981), pp. 979-981.

9. Savchenko, Yu.I., "Hydrodynamic Effects of a Traveling Wave," Bionika 13 (1979), pp. 19-24.

10. Strumolo, G. S., Perturbed Bifurcation Theory for Plane Poiseuille Flow, Ph.D. Thesis, Courant Inst. of Math. Sci., New York U., 1978.

11. Matkowsky, B. J., and Reiss, E. L., "Singular Perturbations of Bifurcations," SIAM J. Appl. Math. 33 (1977), pp.

12. Reiss, E. L., "Imperfect Bifurcation," in Applications of Bifurcation Theory, Ed. by P. Rabinowitz, Academic Press, 1977, pp. 37-71.

13. Hoff, N. J., and Bruce, V. G., Dynamic Analysis of the Buckling of Laterally Loaded Flat Arches," J. Math. and Phys., 32 (1954), pp. 276-288.

14. Kaplan, A., and Fung, Y. C., Buckling of Low Arches or Curved Beams of Small Curvature," NACA-TN 2840, 1952.

15. Cole, J. D., Perturbation Methods in Applied Mathematics, Blaisdell, 1968.

16. Byrd, P. F., and Friedman, M. D., Handbook of Elliptic Integrals for Engineers and Scientists, 2nd Ed., Springer, 1971.

17. Lin, C. C., The Theory of Hydrodynamic Stability, Cambridge Univ. Press, 1955.

18. Orszag, S. A., "Accurate Solution of the Orr-Sommerfeld Stability Equation," J. Fluid Mech. 50 (1971), pp. 689-703.

19. Chen, T. S., and Joseph, D. D., "Subcritical Bifurcation of Plane Poiseuille Flow," J. Fluid Mech. 58 (1973), pp. 337-351.

20. Hall, P., "The Effect of External Forcing on the Stability of Plane Poiseuille Flow," Proc. Roy. Soc. London A 359 (1978), pp. 453-478.

21. Schlichting, H., Boundary-Layer Theory, 6th Ed., McGraw-Hill, 1968.

TABLE I

Disturbance Amplitudes for 2000 Hertz Motions

Material	$\rho/E \times 10^{10}$	$-\varepsilon \times 10^5$ inches			
		$L^2/D^{1/2} = .0046$	$L^2/D^{1/2} = .01$	$L^2/D^{1/2} = .05$	$L^2/D^{1/2} = .1$
Mylar	1.69	.45	.98	4.9	9.8
100 PPI Foam*	3,600	959	2,088	10,440	20,880
RTV**	14,400	3,834	8,350	41,750	83,500

*100 PPI Foam is a polyurethane foam.

**RTV is a silicone rubber.

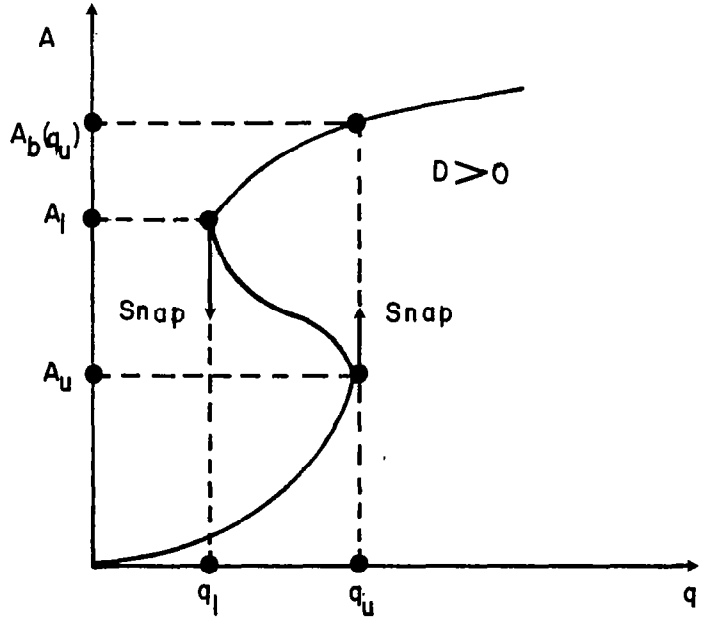

Figure 1

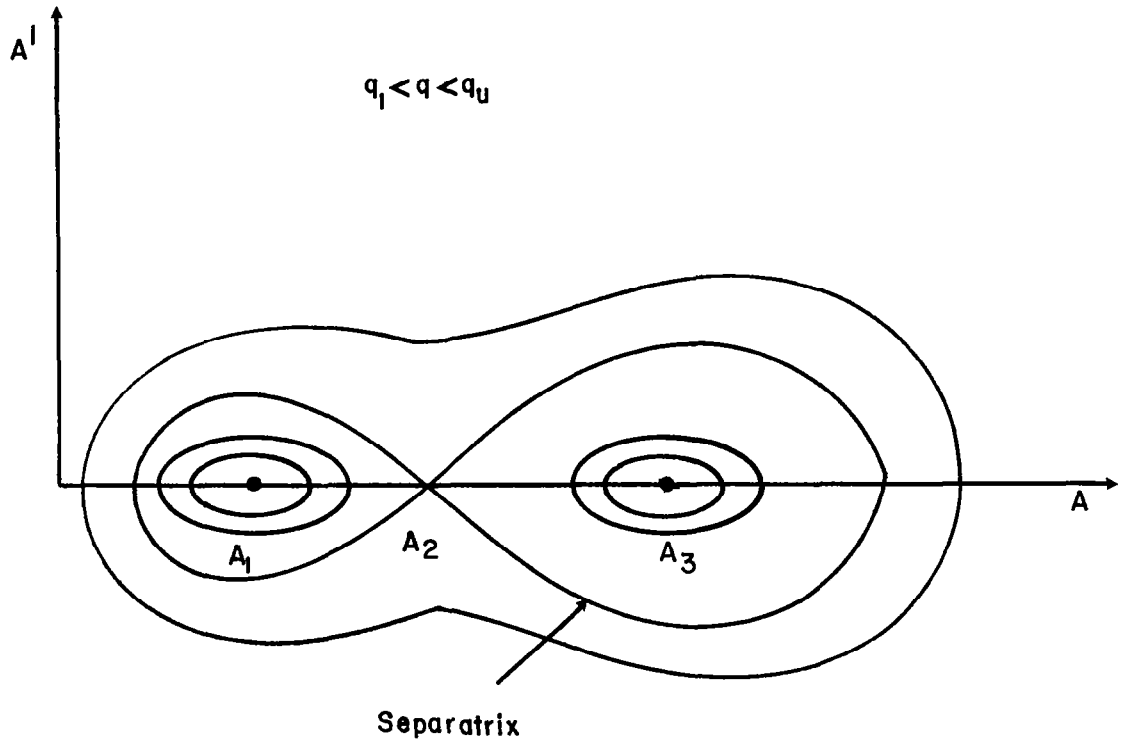

Figure 2

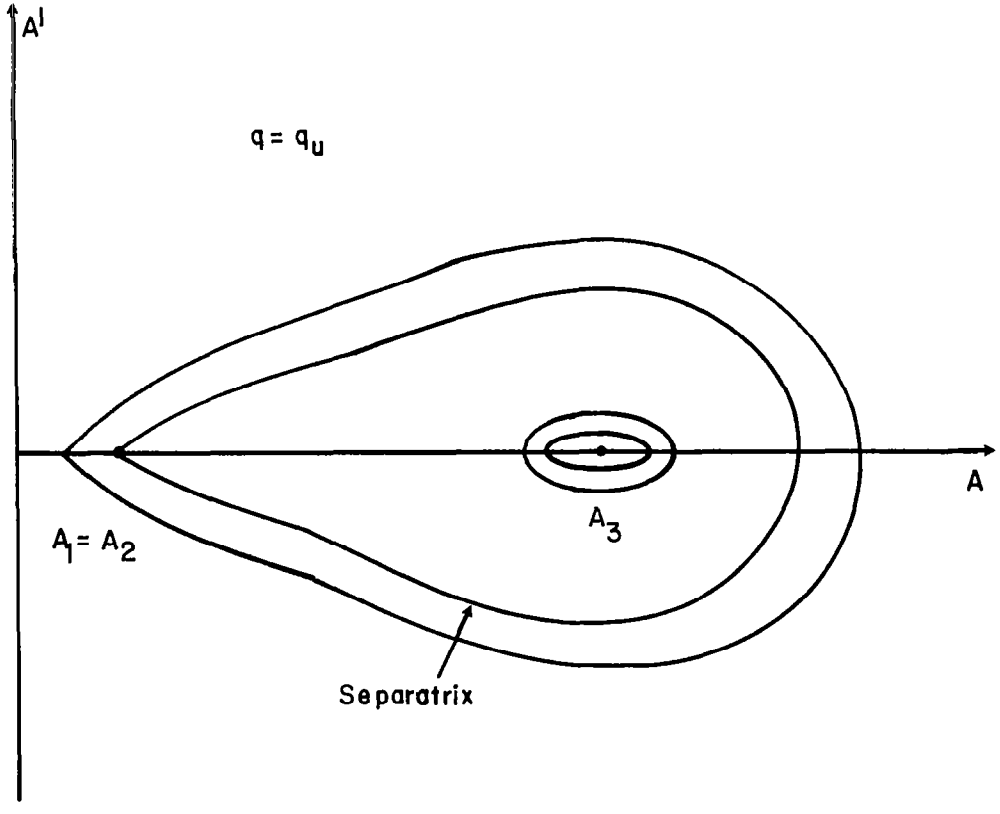

Figure 3

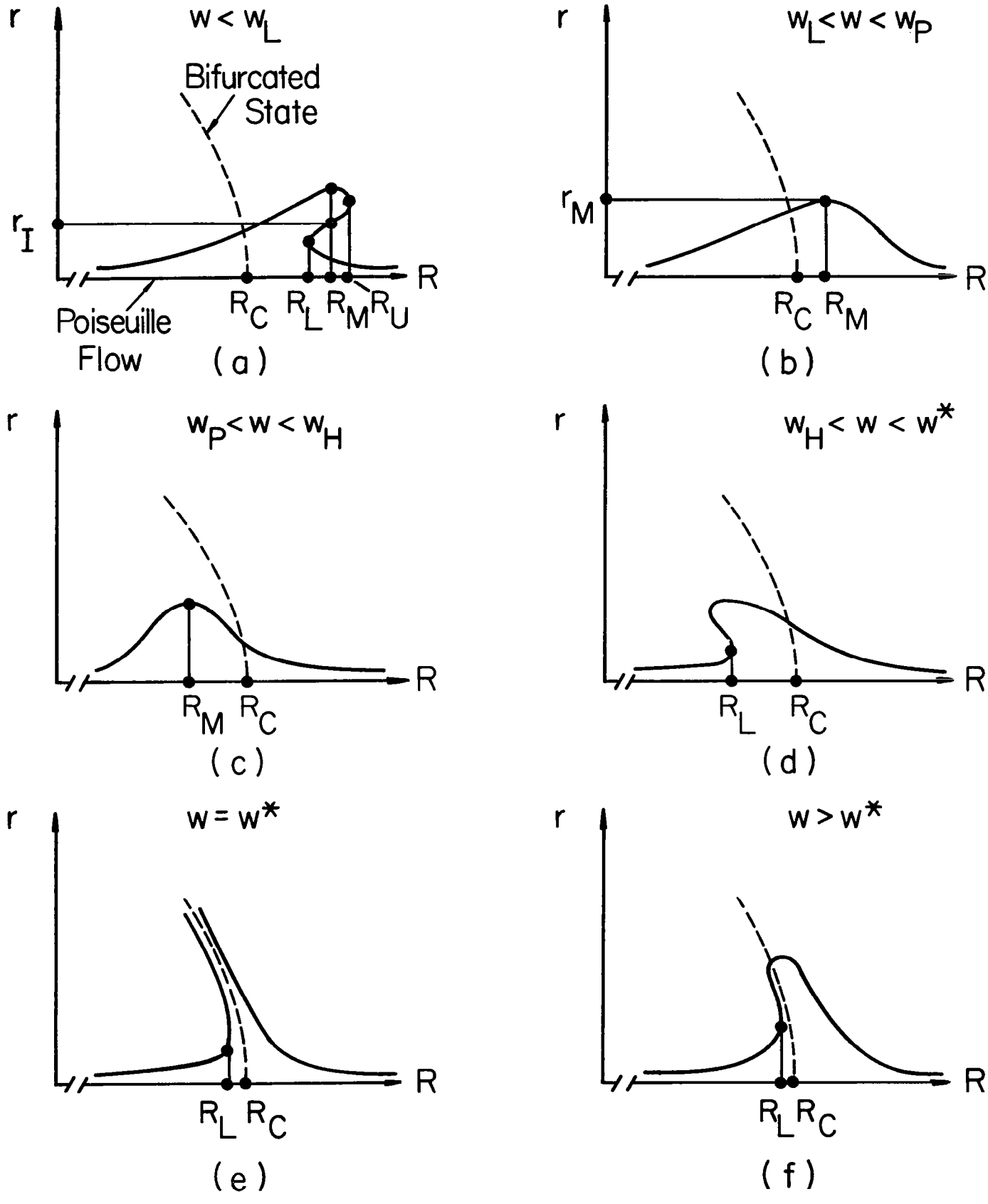
r
w < w_L
Bifurcated
State
r_I
R
Poiseuille
Flow
R_C R_L R_M R_U
(a)
r
w_L < w < w_P
r_M
R
R_C R_M
(b)
r
w_P < w < w_H
R
R_M R_C
(c)
r
w_H < w < w*
R
R_L R_C
(d)
r
w = w*
R
R_L R_C
(e)
r
w > w*
R
R_L R_C
(f)

Figure 4

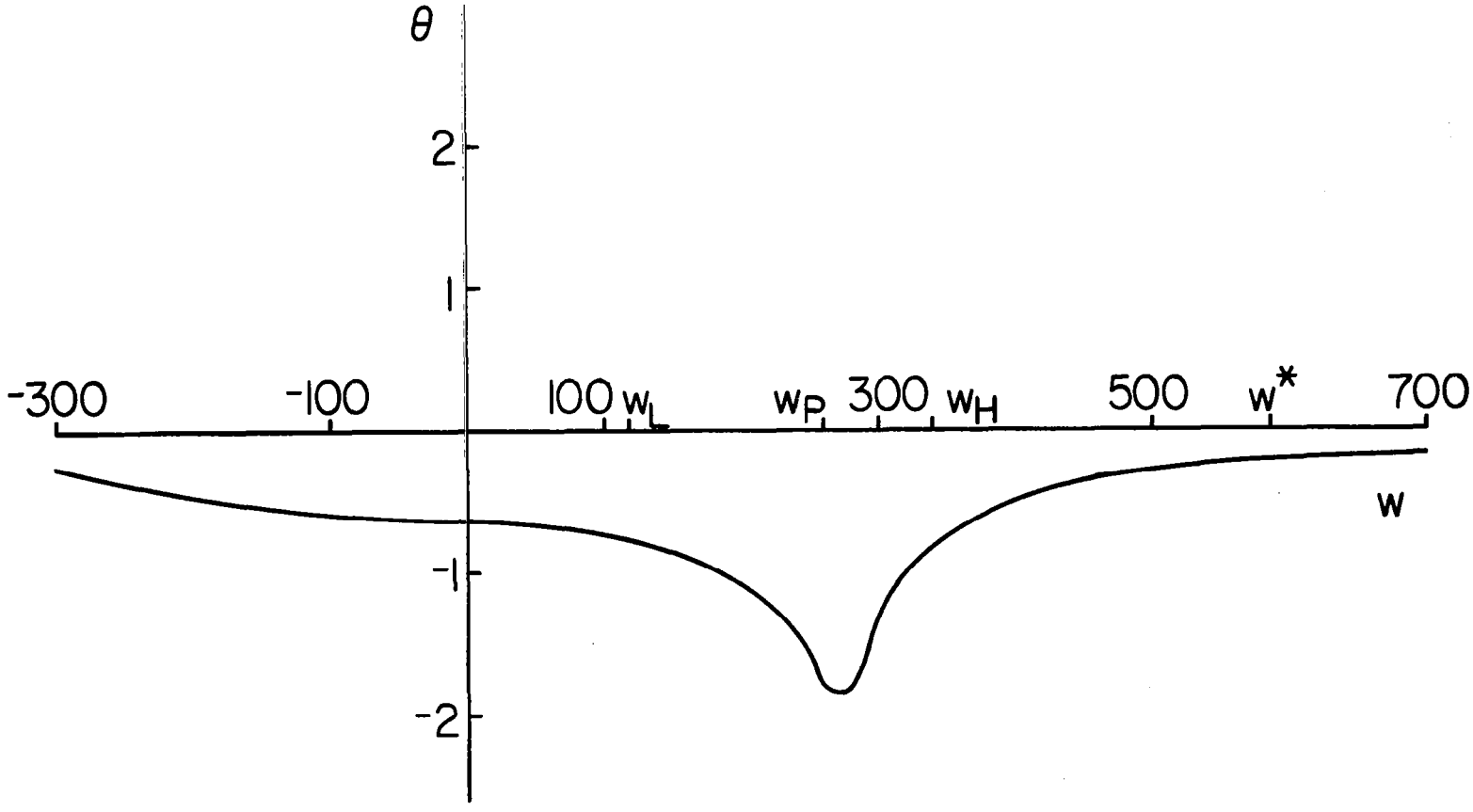

Figure 5

1. Report No.	2. Government Accession No.	3. Recipient's Catalog No.
NASA CR-3628		

4. Title and Subtitle	5. Report Date
A NONLINEAR STRUCTURAL CONCEPT FOR COMPLIANT WALLS	October 1982
	6. Performing Organization Code
7. Author(s)	8. Performing Organization Report No.
Edward L. Reiss	
	10. Work Unit No.
9. Performing Organization Name and Address Applied Institute of Mathematics, Inc. Suite 503 2025 Sherman Avenue Evanston, IL 60201	11. Contract or Grant No. NAS1-14717
	13. Type of Report and Period Covered Contractor Report
12. Sponsoring Agency Name and Address National Aeronautics and Space Administration Washington, DC 20546	14. Sponsoring Agency Code

15. Supplementary Notes

Langley Technical Monitor: Jerry N. Hefner
Final Report

16. Abstract

It is shown that the amplitudes and frequencies of compliant wall motions for drag reduction in accordance with Bushnell's hypothesis might be achieved by using slightly curved walls and the resulting large amplitude motions of snap buckling. A simple structural model of an arch is used in the analysis, and a new asymptotic method is developed. The required wall motions can be obtained by using materials like mylar. In addition, the delay of transition from laminar to turbulent flow by driven walls is studied for Poiseuille channel flow. The walls are driven by a periodic traveling wave. A significant increase in the transitional Reynolds number is obtained by appropriately prescribing the wave length and phase velocity of the wall motion. Previously developed asymptotic methods are used in the analysis.

17. Key Words (Suggested by Author(s))	18. Distribution Statement
Drag Reduction Compliant Walls Driven Wall Fluid-Solid Interaction	Unclassified-Unlimited

19. Security Classif. (of this report)	20. Security Classif. (of this page)	21. No. of Pages	22. Price
Unclassified	Unclassified	40	A03

For sale by the National Technical Information Service, Springfield, Virginia 22161

NASA-Langley, 1982